JOURNAL OF SPACECRAFT AND ROCKETS
Vol. 46, No. 2, March–April 2009

Hypersonic Instability Waves Measured Using Fast-Response Heat-Flux Gauges

Tim Roediger* and Helmut Knauss†
University of Stuttgart, 70569 Stuttgart, Germany
Malte Estorf‡
Technical University of Brunswick, 38106 Brunswick, Germany
Steven P. Schneider§
Purdue University, West Lafayette, Indiana 47906
and
Boris V. Smorodsky¶
Russian Academy of Sciences, 630090, Novosibirsk, Russia

DOI: 10.2514/1.37026

Instability and transition were measured on a 7-degree half-angle sharp cone at zero angle of attack. Surface-mounted heat-flux gauges with a 1-MHz frequency response were mounted in a streamwise array. Experiments were carried out under noisy and quiet Mach-6 flow. Second-mode instability waves and their first harmonics were detected under noisy flow for stagnation pressures ranging from 3.9 to 5.8 bar. Under quiet flow, however, the second mode could only be detected at 8.6 bar due to the much lower amplitude of the fluctuations. The amplification rates were in good agreement with linear stability theory for noisy flow. Under quiet flow, maximum growth rates could not be determined due to the low signal-to-noise ratio.

Nomenclature

A	=	(wave) amplitude
f	=	frequency, Hz
k	=	roughness height, m
M	=	Mach number
p	=	tube pressure, bar, psia
q	=	heat-flux density, W/cm^2
q'	=	fluctuation of heat-flux density, W/cm^2
Re	=	Reynolds number
T	=	temperature, K
U	=	voltage, V
x	=	arc length along surface, m
$-\alpha_i$	=	log growth rate per arc length, 1/m
δ	=	boundary-layer thickness (edge), m
λ	=	wavelength, m

Subscripts

unit	=	per unit length
w	=	wall quantity
0	=	initial quantity

Presented as Paper 638 at the 46th AIAA Aerospace Sciences Meeting and Exhibit, Reno, NV, 7–10 January 2008; received 6 February 2008; revision received 22 December 2008; accepted for publication 23 January 2009.

*Research Assistant, Institute of Aerodynamics and Gas Dynamics, Universität Stuttgart, Pfaffenwaldring 21.

†Senior Scientist, Former Head of High-Speed Laboratory, Institute of Aerodynamics and Gas Dynamics, Universität Stuttgart, Pfaffenwaldring 21. Member AIAA, Retired.

‡Research Assistant, Institute of Fluid Mechanics, Technische Universitaet Braunschweig, Bienroder Weg 3. Member AIAA.

§Professor, School of Aeronautics and Astronautics. Associate Fellow AIAA.

¶Senior Scientist, Institute of Theoretical and Applied Mechanics, Khristianovich Institute of Theoretical and Applied Mechanics, Institutskaya str. 4/1.

I. Introduction

ONE of the key factors for the aerodynamic design of hypersonic flight vehicles involves the consideration of surface heat loads. The process of laminar to turbulent boundary-layer (BL) transition is accompanied by large changes in surface heat transfer and skin-friction drag. This effect has a dramatic influence on aerodynamic coefficients, stability, and structural design of such vehicles. Yet the physics of the transition process associated with the growth of disturbances in the BL is still poorly understood. Conical boundary layers are prevalent in many hypersonic vehicles and stability measurements on sharp cones have been conducted since the 1970s. Schneider [1] gives a review of experimental and numerical studies on the subject and provides an overview of instability mechanisms on circular cones, including a comprehensive list of references. It is stated that the second-mode instability is dominant at hypersonic speeds in symmetric flows, at least in simple cases like the one of circular cones. The instability is influenced by several effects like bluntness, wall cooling, surface roughness, and acoustic noise. The latter effect is the subject of the current investigation. Acoustic noise is radiated from turbulent BLs on the walls of hypersonic ground-testing facilities. Several investigations have been carried out in quiet and noisy flow at various hypersonic Mach numbers in different wind tunnels. Most of the measurements were conducted using hot-wire anemometry. There are several drawbacks to this technique: Besides the limited frequency response and mechanical strength of hot wires, their downstream influence excludes simultaneous streamwise amplitude measurements. A nonintrusive technique for simultaneous measurements of instabilities using streamwise arrays would permit determination of growth rates. Currently, the laser-differential interferometer (LDI) is the only optical technique able to measure high-frequency instability waves, and an array of LDIs would be difficult to implement [2]. Therefore, surface-mounted measurement techniques with high spatial and temporal resolution are very attractive for this purpose. Recently, the fast surface-pressure sensors pioneered by Fujii [3] were used to measure second-mode instability waves under quiet and noisy flow in two Mach-6 Ludwieg tubes. These gauges possess a very good temporal and reasonable spatial resolution. However, they only detect pressure fluctuations and not absolute values, which would be of interest for comparisons with numerical computations of the base flow. In addition, the study of instability waves in the high-frequency range is

Table 1 Specification of installed ALTPs

Position, no.	Arc length x, mm	ALTP, serial number	Sensitivity s (incl. absorpt.), $\mu V/(W/cm^2)$	Max. roughness height k, mm
11	370	941	87.4	0.174
12	395	942	126.7	0.163
13	420	944	83.5	0.154
14	445	943	77.6	0.145

very challenging, and experiments showing fluctuation data of different physical quantities are very desirable. Certain techniques might prove more useful due to a variation of eigenfunction properties in different flowfields. Therefore, a surface measurement technique with sufficient temporal and spatial resolution detecting fluctuations of heat flux per unit area (more precisely heat-flux density) is used in the present paper. The atomic layer thermopile (ALTP) is a fast-response heat-flux gauge with a spectral resolution near 1 MHz. The gauge can be used to capture the fluctuations in heat flux, as well as the mean heat flux at the wall. The present work focuses on the detection of instability waves, determination of their spatial growth rates, and comparison of the experimental results with linear stability theory computations in a conical BL at Mach 6 under noisy and quiet flow.

II. Experimental Setup

A. Facility

The present experiments were conducted in the Mach-6 Quiet-Flow Ludwieg Tube of Purdue University. A detailed description of the facility can be found in Schneider [5] and Juliano et al. [6]. The Ludwieg tube operates with laminar nozzle BL resulting in quiet hypersonic flow conditions up to stagnation pressures of approximately 145 psia (∼10 bar). Noisy flow is achieved for a pressure range up to 270 psia (∼18.6 bar). To determine the freestream conditions, the driver-tube pressure was measured at the entrance of the contraction and the temperature was determined at the end of the driver tube before every run. The temperature measurement is subject to uncertainty due to stratification and axial temperature differences in the tube. Therefore, a more accurate procedure [4] based on the method of characteristics is used to determine the temperature during the whole run. By means of this method, the uncertainty of the air temperature at the model is estimated to ±0.8% and the uncertainty of the pressure is about ±0.2%. The Mach number is determined by pitot pressure measurements as $M = 5.8$ in noisy flow and $M = 6$ in quiet flow conditions. The uncertainty of the test section Mach number is approximated by ±2%. This leads to an uncertainty in the calculation of the Reynolds number in the test section of approximately ±4%.

The freestream noise level is ∼0.05% in quiet flow when the nozzle BL remains laminar. In conventional (noisy) operation, the turbulent nozzle BL increases the noise level to ∼3%.

B. Cone Model

A 7-deg half-angle cone with a sharp nose tip was installed in the test section. The 500-mm-long cone is made from aluminum. It allows the installation of up to 14 gauges along a generator starting at $x = 100$ mm from the nose tip, with an axial spacing of 25 mm in the downstream direction (see Fig. 1). Contoured blind stoppers replace unused gauge positions. For better installation, the cone consists of two pieces and an exchangeable nose tip. The diameter of the tip was estimated to be about 6 μm by means of a microscope.

The rear sting mount of the cone is made from steel to permit firm and accurate installation of the model. Yet the angle of attack of the cone model could not be verified (e.g., by optical methods), due to limited accessibility. Therefore, the model was rotated on its rear mount at angles of 90, 180, and 270 deg. A slight shift in the maximum frequency of the second mode was visible for repeated runs at the same nominal conditions. The results document a small angle of attack with the sensor array being slightly windward (perhaps 0.1 deg or less).

C. Instrumentation

The heat-flux density fluctuation measurements were performed by use of a novel fast-response heat-flux gauge called the atomic layer thermopile. The very fast frequency response of the sensor allows for highly time-resolved heat-flux measurements up to the 1 MHz range. Its working principle is based on the transverse Seebeck effect. The output signal is directly proportional to heat-flux density and has a linear characteristic in the 10 W/m^2 to 1×10^6 W/m^2 range. For a detailed description of the working principle, structure, and calibration procedure of the sensor, the reader is referred to Roediger et al. [7].

An array of four single-point ALTP modules was installed at positions $x = 370, 395, 420$, and 445 mm (see Table 1). The gauge at position $x = 420$ mm was damaged during the experiments and is not considered in the following. The active area of the ALTP gauges used in the present experiments is 2×0.4 mm^2, limiting the spatial resolution in the streamwise direction to 0.4 mm. The gauges are calibrated by exposure to laser light radiation and have a sensitivity between 83 and 127 $\mu V/(W/cm^2)$ (see Table 1). The total uncertainty of the calibration procedure is estimated as 5.5% [7]. The housing of the module is made of a ceramic insulator (MACOR) to achieve a mainly one-dimensional heat flux through the substrate. The module has a flat surface with a diameter of 8 mm. Therefore, it could not be perfectly flush mounted in the circular cone and only its streamwise diameter was aligned with the cone surface. The maximum roughness height created by the modules varied from $0.145 \leq k \leq 0.174$ mm depending on the position of the sensor (see Table 1). The influence of the roughness created by the sensor module was found to be marginal in similar hypersonic cone experiments [8].

Low-noise amplifiers with a nominal gain of 5000 and signal conditioning were used for the amplification of the ALTP sensor signals. The miniature amplifiers were installed inside the cone model to minimize electronic interference.

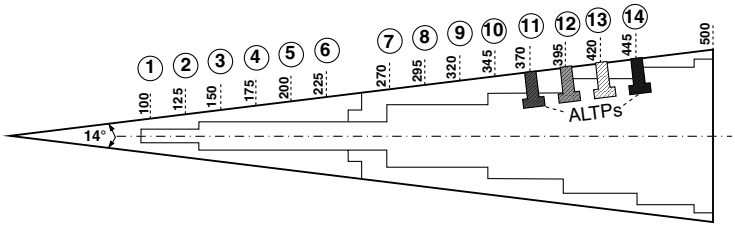

Fig. 1 Schematic of circular cone model with installed ALTP gauges.

III. Data Analysis

A. Data Acquisition and Processing

A four-channel digital oscilloscope (Tektronix DPO 7054) was used for data acquisition. The signals were captured at a sampling rate of 4 MS/s in high-resolution mode. According to the manufacturer, the mode results in an effective resolution of 11 bits and the data are saved in a 16 bit format.

A time trace of 5 s was recorded for each run, consisting of a 0.5 s reference trace before the start of the tunnel and 4.5 s of usable measuring time history. A time interval of 0.2 s length (800,000 samples) was extracted at the same measuring time of 2 s (1.5 s after the start of the tunnel) for the runs in noisy flow conditions. Under quiet flow, a larger time interval of 0.4 s length (1.6×10^6 samples) was used. The beginning of the extracted sample was slightly adjusted within a window 1.5 ± 0.1 s after the start of the tunnel to exclude windows of occasionally noisy flow that are believed to be due to turbulent spots passing on the nozzle wall [6]. The heat-flux values were calculated from voltage fluctuations using the specific calibration factors of the sensors. The resulting heat-flux signals were divided into overlapping windows with an constant size of 1000 samples each and an overlap of 400 samples. The windows were multiplied with a normalized exact Blackman window and Fourier transformed. Afterward, the amplitude spectra are averaged over all windows.

In addition, the background noise spectrum was calculated from a sample of the same size taken from the data measured before the start of the tunnel. It is processed in the same way as described earlier and subtracted from the spectrum during the run. Hence, the uncorrelated electronic noise and disturbances are eliminated from the resulting amplitude spectra. Figure 2 depicts the data processing, showing the noise spectrum before the run, the measured spectrum during the run, and the resulting spectrum after the power spectral subtraction of the noise. At some frequencies, the spectral subtraction of the background noise yielded negative amplitude values. These values were set to zero. It remains to be verified whether such a correction is the best or most appropriate method.

B. Amplitude-Frequency Response Correction

To account for the amplitude-frequency response (AFR) characteristics of the whole system consisting of the specific ALTP gauges and amplifier, all spectral data presented in the following are corrected by experimentally determined AFRs. The characteristics are obtained from dynamic laser beam calibration using the modulated output of a diode laser (Sony SLD 1332 V) in a frequency range between 1 kHz and 1 MHz. The output of the laser is monitored by a photodiode with a time constant of about 50 ns. Therefore, a reference signal with sufficient temporal resolution for such a high-frequency dynamic calibration is produced. The time signals of the diode and the ALTP were captured with a digital oscilloscope (LeCroy 9361) and 600 samples were averaged into the internal memory. For additional information on the dynamic calibration procedure and setup, the reader is referred to Roediger et al. [7] and Knauss et al. [9].

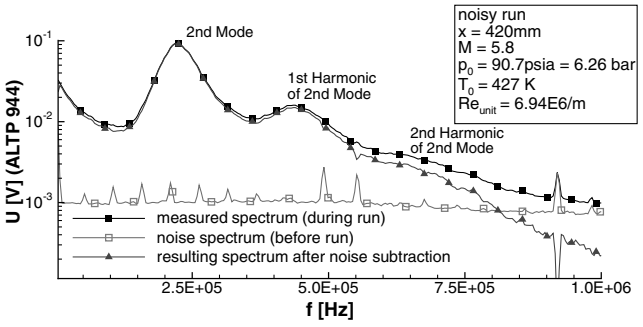

Fig. 2 Data processing and noise subtraction for sample ALTP spectrum.

Figure 3a shows the AFR resulting from the normalized amplitude ratios of the monitor diode A_{diode} and ALTP A_{ALTP} for two ALTPs. The repeatability of the amplitude ratios is excellent, however, the uncertainty of the AFR increases with rising frequency due to the limited signal-to-noise ratio of the ALTP signal. Therefore, the signal-to-noise ratios of the diode and the ALTP signal are shown in Fig. 3b. The signal quality of the reference is sufficient across the entire frequency range. However, the signal-to-noise ratio of each individual ALTP limits the accuracy of the AFR characteristics by approaching the electronic noise level. In Fig. 3c, the phase difference ($\phi_{\text{diode}} - \phi_{\text{ALTP}}$) between the diode and ALTP signal is displayed. The error bars given in the diagram result from the limited sampling rate of the oscilloscope restricting the temporal resolution of the captured sine wave signals.

Figure 3a shows the individual dynamic characteristics of two ALTPs. For a prescribed attenuation of -3 dB (equivalent to $A_{\text{ALTP}}/A_{\text{ref}} = 0.71$), a value of $f \approx 150$ kHz can be assigned for ALTP 942 and $f \approx 200$ kHz for ALTP 944. It shall be mentioned that the dynamic characteristics of the third ALTP used in the experiments (ALTP 941) are very close to the one of ALTP 942. For the ALTP with larger time constant (ALTP 942) the phase difference continuously decreases and reaches a maximum value of -65 deg at $\sim$500 kHz. The phase difference for ALTP 944, however, decreases at a much slower rate and approaches values below 30 deg only for frequencies beyond $\sim$400 kHz. The phase relation clearly correlates with the time constant of the ALTP films. In general, the differences of dynamic properties are mainly related to a variation of film thickness resulting from certain manufacturing tolerances [9].

For the correction of the spectral data, the individual AFRs (Fig. 3a) are used. Figure 4 demonstrates the effect of the AFR correction on the spectrum (after noise subtraction) shown in Fig. 2. The AFR corrected amplitude spectra allow the accurate calculation of wave amplitudes and amplification rates.

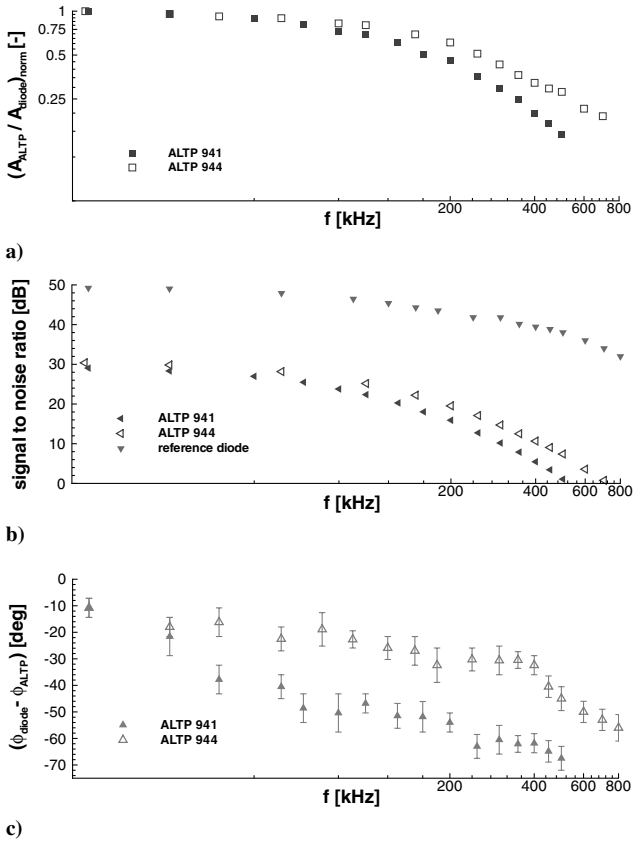

Fig. 3 Dynamic characteristics obtained by laser calibration a) amplitude-frequency response, b) signal-to-noise ratio, and c) phase.

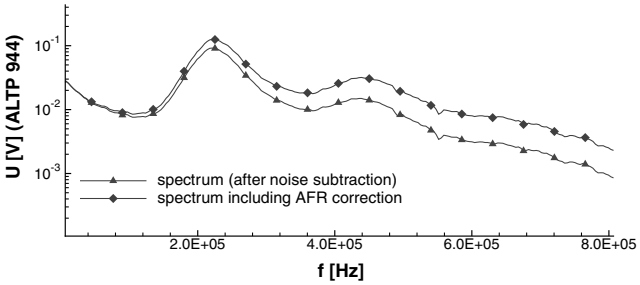

Fig. 4 Demonstration of amplitude-frequency response correction.

C. Spatial Amplitude Growth

The definition for the amplification rate in the x direction is given by Mack [10] as

$$-\alpha_i = \left(\frac{1}{A}\right)\left(\frac{\mathrm{d}A}{\mathrm{d}x}\right) \tag{1}$$

with negative values of α_i denoting amplification and A referring to the wave amplitude. For the case of two streamwise single-point sensors at positions 1 and 2 with specified spatial distance $(x_2 - x_1)$, the amplitude ratio yields

$$\frac{A_2}{A_1} = e^{-\int_1^2 \alpha_i \,\mathrm{d}x} \tag{2}$$

If α_i is constant, exponential amplitude growth can be assumed and the integral in the exponent can be simplified to

$$\frac{A_2}{A_1} = e^{-\alpha_i (x_2 - x_1)} \tag{3}$$

Finally, the spatial amplification rate can be calculated from

$$-\alpha_i = \frac{\ell_n (A_2/A_1)}{x_2 - x_1} \tag{4}$$

Equation (4) is used for the calculation of the amplification rates between the single-point sensors in the following experiments. It must be noted, however, that this assumption is only of limited validity because the distance between the sensors is fairly large and several times the wavelength of the investigated instability waves. Especially in regions of large changes of the amplification rate (compare stability diagrams in Sec. V), this assumption results in an averaged amplitude ratio and might deviate from predictions of local linear stability theory.

IV. Experimental Results

A. Noisy Flow Condition

Figure 5 shows the amplitude spectra at the fixed location $x =$ 395 mm (ALTP 942) for a variation of unit Reynolds number. The diagram describes the shift of the transitional regime across a fixed position on the cone surface. The diagram visualizes the successive stages of BL transition detected by fluctuation of heat-flux density at the wall under noisy flow.

Figures 6a–6c show the obtained amplitude spectra for a fixed unit Reynolds number at the three consecutive sensor positions. All diagrams clearly reveal the frequency shift of the second-mode instability to lower frequencies in the downstream direction due to the increasing BL thickness along the cone. The wavelength of the second mode is proportional to the BL thickness and is roughly approximated by $\lambda \approx 2\delta$. The first peak in the amplitude revealing the second mode is situated in a frequency range of 180–220 kHz. In addition, a first harmonic of the second-mode instability was captured in a frequency range between 300–400 kHz for certain stages of BL transition. A weak residual of a second harmonic of the second-mode instability is possibly visible in some amplitude spectra (ALTP 944 in Fig. 4) captured by an ALTP with very good AFR characteristic.

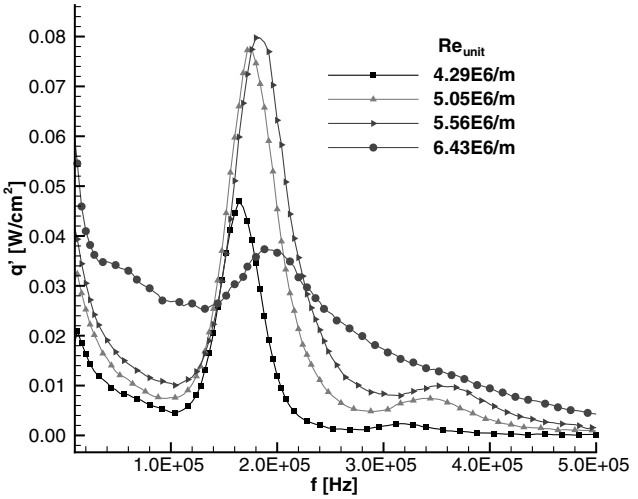

Fig. 5 Amplitude spectra (AFR corrected) for unit Reynolds number variation at fixed sensor location $x = 395$ mm.

At the lowest realized unit Reynolds number $Re_{\mathrm{unit}} = 4.29\mathrm{E}6/\mathrm{m}$, the amplitudes of the second-mode instability rise in the downstream direction. The amplitude spectra seems to show that the BL is already transitional at this Reynolds number, because the amplitudes increase in a wide frequency range above and below the second mode.

At a slightly higher unit Reynolds number (Fig. 6b), the amplitude of the second mode at the rear gauge position starts to decrease and the first harmonic disappears. It shows that the BL is close to the turbulent state. At the highest unit Reynolds number $Re_{\mathrm{unit}} = 6.43\mathrm{E}6/\mathrm{m}$ (Fig. 6c), the second mode finally disappears completely at $x = 445$ mm and the spectrum is characteristic of a turbulent BL state.

Figure 7 demonstrates the calculation of the amplification rates for the case of the lowest realized unit Reynolds number $Re_{\mathrm{unit}} = 4.29\mathrm{E}6/\mathrm{m}$ and therefore the earliest stage of BL transition. The ratios are calculated from the amplitude spectra (note logarithmic scale) without any analytical approximation of the spectrum. The results show not only the amplification rates of the second mode but also the rates in the extended frequency range of its first harmonic. The maximum rate of the second mode is about $25/\mathrm{m}$ at 125 kHz. The amplification rate of the first harmonic is even a bit higher and reaches values of $\sim 27/\mathrm{m}$ at 280 kHz. In addition, the spectrum in the frequency range below the second mode is slightly amplified. These observations indicate the transitional character of the BL and the nonlinear effects already present in the BL. Nonlinear processes might also be caused by roughness effects due to the flat sensor module that lead to the creation of disturbances in the BL. A similar behavior was observed in cone experiments in a comparable unit Reynolds number range but at adiabatic wall conditions (Knauss et al. [9]). This effect has to be studied in further detailed investigations of roughness elements.

B. Quiet Flow Condition

Figure 8 shows the second-mode instability detected at a driver-tube pressure of 124.4 psia (8.58 bar). The initial pressure of the run is close to the upper limit where quiet flow can currently be achieved in the Ludwieg tube. The second mode could not be detected at lower unit Reynolds numbers, because the fluctuations are more than an order of magnitude smaller under quiet flow, and the limited signal-to-noise ratio of the ALTP sensors cannot detect them. Because the second-mode instability could only be detected at higher stagnation pressures, it is not possible to compare the wave amplitudes at the same Reynolds number in quiet and noisy hypersonic flow at natural disturbance levels. However, the comparison of second-mode wave amplitudes in quiet flow conditions at $Re_{\mathrm{unit}} = 8.94\mathrm{E}6/\mathrm{m}$ and in noisy flow at $Re_{\mathrm{unit}} = 4.29\mathrm{E}6/\mathrm{m}$ shows that their amplitudes in quiet flow are ~ 12 times smaller than in noisy flow conditions at the same

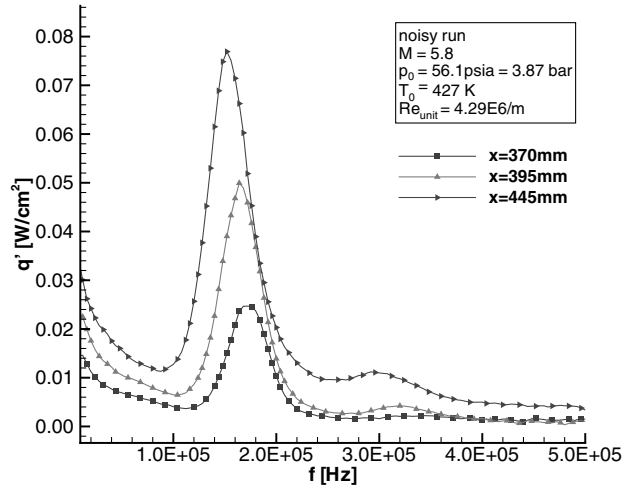

a)

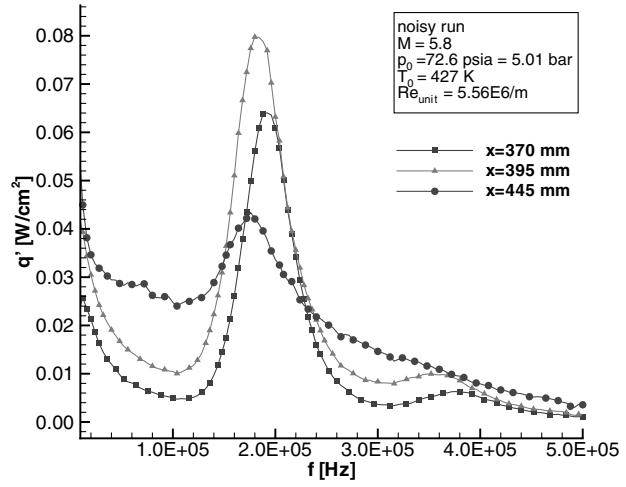

b)

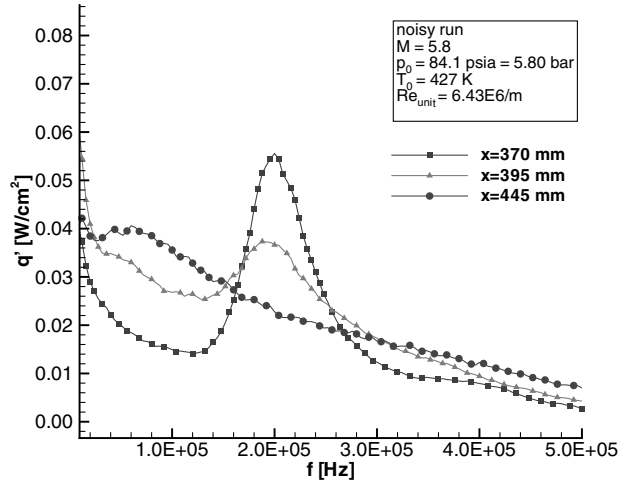

c)

Fig. 6 Amplitude spectra (AFR corrected) for a) $Re_{\text{unit}} = 4.29\text{E}6/\text{m}$, b) $Re_{\text{unit}} = 5.56\text{E}6/\text{m}$, and c) $Re_{\text{unit}} = 6.43\text{E}6/\text{m}$.

x location. A direct comparison of the amplitudes would only be possible by using linear stability theory to compute the amplification between the two states.

The fluctuations of heat-flux density at the wall are in the milliwatt per square centimeter range and mark the lower limit of detectable heat-flux density by means of the ALTP. Experiments with a higher ratio of total temperature to wall temperature are clearly desirable to improve the signal-to-noise ratio.

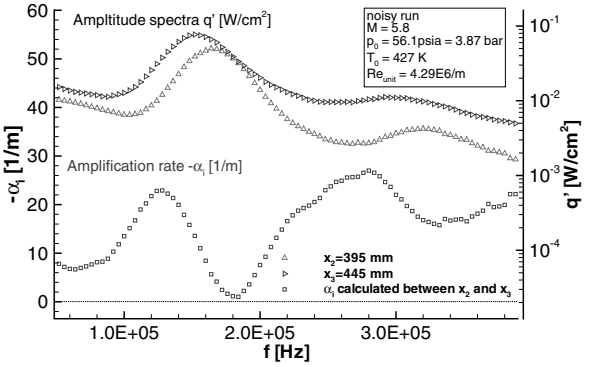

Fig. 7 Amplification rate calculated between positions $x = 395$ and 445 mm for noisy flow.

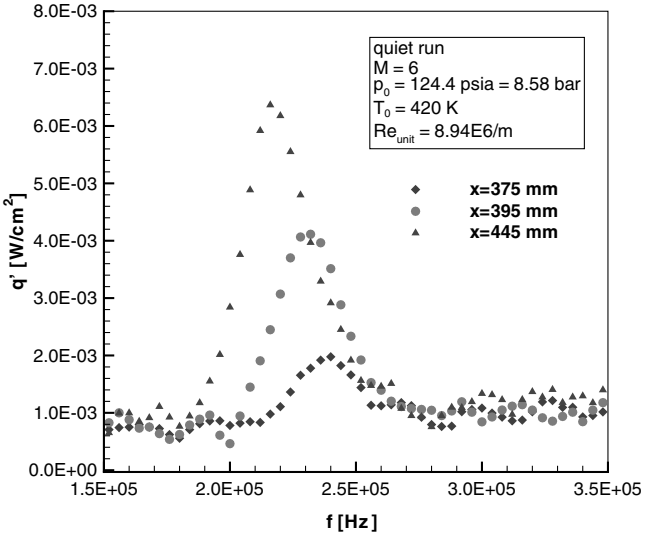

Fig. 8 Amplitude spectra (AFR corrected) for $Re_{\text{unit}} = 8.94\text{E}6/\text{m}$ (run 39).

Figure 9 demonstrates the calculation of growth rates from amplitude spectra at locations $x = 395$ and $x = 445$ mm (note logarithmic scale). Amplification rates are subject to high uncertainty, especially on the left edge of the second-mode peaks: the region of highest amplification rates. Because of the low amplitudes of the fluctuations, the second-mode peak of the upstream sensor (right bell) drops faster below the background noise level than the peak of the downstream sensor (left bell). The calculation of

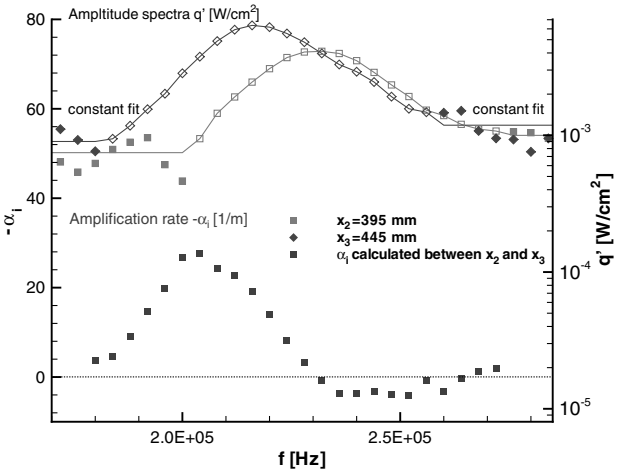

Fig. 9 Amplification rates between positions $x = 395$ and 445 mm for quiet flow (run 39).

ratios in this region is very sensitive. Low signal-to-noise ratios or analytical fitting in this region can produce arbitrarily high maximum amplification rates. Therefore, the spectrum to the left and right of the second-mode bells is approximated by a constant fit as shown in Fig. 9. The constant value to the left of each bell corresponds to the mean value of the background noise (filled symbols) in a frequency range between 150 kHz and the beginning of the second-mode peak (hollow symbols). On the right-hand side, the constant results from the mean value in the frequency range extending from the right edge of the peak up to 340 kHz. The second-mode bell itself is not approximated by any analytical function. The maximum amplification rate of sample run 39 is about 28/m. This value is the maximum rate observed in three repeated runs at the same nominal conditions. The other runs only reached values of 16 and 18/m. However, the background noise level of these runs was slightly higher. This indicates the uncertainty of the determined maximum amplification rates in quiet flow. The averaged amplification rates of these three repeated runs will be discussed later.

V. Comparison of Experimental Results with Linear Stability Theory

Linear stability theory (LST) calculations are carried out for comparison with the experimentally obtained amplification rates at corresponding unit Reynolds numbers under quiet and noisy flow. The axisymmetric conical BL of a sharp cone at zero angle of attack was computed by means of self-similar flat-plate compressible boundary-layer equations using the Lees–Illingworth transformation [11]. Wall temperature, Prandtl number, and specific heat ratio are assumed to be constant. Sutherland's law is used for the viscosity. In addition, the flow is assumed uniform in the streamwise flow close to the cone surface downstream of the attached shock. The outer inviscid flow properties on the cone surface were determined by means of the numerical integration of Taylor–Maccoll equation [12]. Local linear stability analysis of the BL is performed in the framework of the eigenvalue problem for Lees–Lin equations [13], which have been integrated numerically by means of the method of orthonormalizations [14]. Spatial growth rates of the instability waves are determined by eigenvalues as functions of the flow stagnation parameters and wave frequency.

Figures 10 and 11 show the cone BL stability diagrams for the noisy and quiet run, respectively. The diagrams display the spatial amplification rate contours in the plane of dimensional frequency versus distance x from the cone tip. Shaded areas correspond to unstable domains with respect to 2-D first- and second-mode instability waves (lower and upper regions, respectively). It can be noted that regions of instability of first and second modes are separated from each other in both diagrams. The region of second-mode instability is represented by a relatively narrow frequency band which trends downward quite fast with increasing x. The location of the ALTP sensors used for the calculation of the experimental rates are displayed by vertical lines. Looking at these cross sections, the sensors at the two x locations should register peaks in the fluctuations of wall heat-flux density at different frequencies. Probes positioned further downstream will detect a spectral peak at lower frequencies. Please note that the first mode possesses 1-order-of-magnitude lower growth rates in comparison with the second-mode instability.

Figures 12a and 12b display the experimentally obtained and the calculated 2-D spatial amplification rates in noisy and quiet flow, respectively. The LST rates are evaluated at a location in the middle of the two probe positions ($x = 420$ mm) as a first approach (integrated amplifications should be used for more accurate comparison). The magnitudes of the measured and predicted maximum growth rates in noisy flow are in good agreement. The slightly lower experimental data may be due to the small angle of attack, as described in Sec. II, or might result from an increase in wall temperature during the run. A rise in wall temperature stabilizes the second-mode instability and could decrease the maximum amplification rates. The magnitude of this effect is estimated for

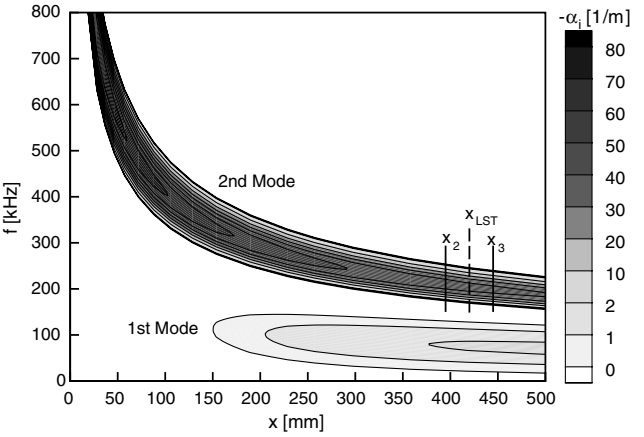

Fig. 10 Stability diagram for noisy run (flow conditions: $M = 5.8$, $p_0 = 56.1$ psia $= 3.87$ bar, $T_0 = 427$ K, $T_w = 310$ K, $Re_{\text{unit}} =$ 4.29E6/m).

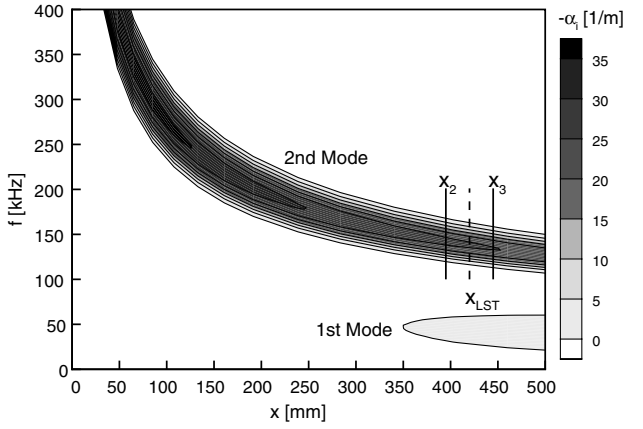

Fig. 11 Stability diagram for quiet run (flow conditions: $M = 6$, $p_0 = 124.4$ psia $= 8.58$ bar, $T_0 = 420$ K, $T_w = 310$ K, $Re_{\text{unit}} =$ 8.94E6/m).

the quiet run in Fig. 12b. The results show that a wall temperature rise of 33 K leads only to a decrease of maximum growth rate by ~9%. In addition, superposition of 3-D modes leads to lower amplification rates in comparison with LST, which assumes here only the existence of 2-D modes. Investigations with a three-dimensional sensor array on the surface of a cone are necessary to confirm the absence of 3-D modes. Furthermore, lower experimental growth rates were also previously reported (see review by Stetson and Kimmel [15] and references therein). The disagreement was suspected to originate from the large nonlinear nature of the waves measured under noisy flow. Yet Fig. 7 shows that the growth rate of the first harmonic is only marginally higher than the one of its fundamental. Inaccuracies in the Sutherland law may also be responsible.

In quiet flow, the average experimentally determined maximum rates are significantly lower. As stated in Sec. IV.B, scatter in the three measurements was large, and the maximum rates could not be reliably determined due to the low amplitude of the fluctuations and the high uncertainty in the determination of amplification rates on the left edge of the second-mode bells. Hence, the maximum value is situated in the frequency range that could not be properly resolved by the measurements.

Both diagrams show that the frequency of the second mode predicted by the calculations is slightly higher. The experimentally determined maximum growth rate in noisy flow is ~10 kHz below the calculated one, or about 8%. This effect is very likely caused by the small angle of attack of the cone, because the wavelength of the second mode scales approximately with the boundary-layer thickness. In quiet flow, the frequency of the maximum growth rate in measurement and calculation seems to coincide well.

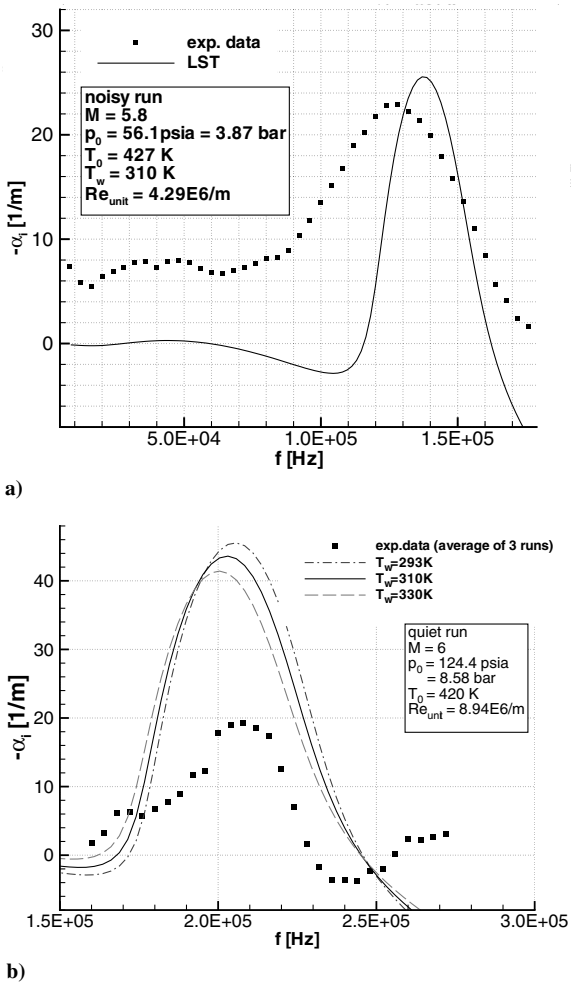

Fig. 12 Comparison of experiments and computations under a) noisy flow, and b) quiet flow.

However, the maximum is suspect to a high uncertainty as stated previously and the more credible right branch of the curve shows a similar 10 kHz shift in frequency. Extrapolating by assuming a behavior similar to the theoretical growth rate would place the measured maximum at lower frequency than the theoretical curve, as in noisy flow. The bandwidth of amplified frequencies in noisy flow varied significantly from the predicted one. The frequencies below and above the second mode are already amplified. As stated in Sec. IV.A, these observations might indicate the presence of nonlinear effects and point out the transitional character of the BL.

VI. Conclusions

Hypersonic transition was studied on a 7-deg half-angle sharp cone under noisy and quiet flow. A streamwise array of fast-response heat-flux gauges was used to determine spatial amplification rates of instability waves. The gauges possess an excellent spatial resolution of 0.4 mm and cover a frequency range up to 1 MHz.

In noisy flow, the consecutive stages of boundary-layer transition could be documented by quantitative amplitude spectra of heat-flux density at the wall. The amplitude-frequency response characteristics of the measurement system are taken into account to determine absolute values of wave amplitudes. The dominant second mode and its first harmonic showed similar growth rates during the early stages of boundary-layer transition. Measured maximum growth rates for the second mode were in very good agreement with those calculated using linear stability theory. The difference in the amplified range of second-mode frequencies is possibly due to a small angle of attack. The measured spectral range of amplified frequencies was more broad than the one predicted by linear stability theory, which might indicate the presence of nonlinear effects.

Under quiet flow, the calculation of growth rates in the region of maximum amplification rates is subject to high uncertainty due to the low amplitude of second-mode waves. Therefore, the measured maximum growth rates do not match the computations. The bandwidth of the amplified frequencies is, however, in good agreement. The measured amplitude of the fluctuations in quiet flow was in the milliwatt per square centimeter range, which clearly marks the lower limit of detectable heat flux per unit area by means of the ALTP. Experiments with a higher ratio of total temperature to wall temperature are needed to improve the signal-to-noise ratio.

The ALTP is of special interest for transition research in hypersonic facilities with high stagnation enthalpy where conventional measurement techniques like hot wires cannot be used. Furthermore, the comparison of growth rates detected by fast-response pressure and ALTP heat-flux gauges to study the eigenfunction properties in different flowfields is certainly of interest for future investigations. The ALTP might also prove useful to measure instability waves in flight.

Acknowledgments

This research was supported by the German Research Foundation within the project KN 490/2. The help and advice of the team at the Mach-6 Quiet-Flow Ludwieg Tube of Purdue University is gratefully acknowledged. The authors from the Institute of Aerodynamics and Gas Dynamics would like to thank S. Wagner (Director Institute of Aerodynamics and Gas Dynamics, retired), E. Kraemer (Director Institute of Aerodynamics and Gas Dynamics), and U. Gaisbauer (head of gas dynamics research group, Institute of Aerodynamics and Gas Dynamics) for their administrative support. In addition, the authors greatly appreciate the cooperation with J. Betz (FORTECH) for the design of specific atomic layer thermopile prototypes.

References

[1] Schneider, S. P., "Hypersonic Laminar-Turbulent Transition on Circular Cones and Scramjet Forebodies," *Progress in Aerospace Sciences*, Vol. 40, Nos. 1–2, 2004, pp. 1–50. doi:10.1016/j.paerosci.2003.11.001

[2] Salyer, T. R., Collicott, S. H., and Schneider, S. P., "Feedback Stabilized Laser Differential Interferometry for Supersonic Blunt Body Receptivity Experiments," AIAA Paper 2000-416, Jan. 2000.

[3] Fujii, K., "Experiment of Two-Dimensional Roughness Effect on Hypersonic Boundary-Layer Transition," *Journal of Spacecraft and Rockets*, Vol. 43, No. 4, 2006, pp. 731–738. doi:10.2514/1.17860

[4] Estorf, M., Schneider, S. P., Johnson, H. B., and Hein, S., "Surface-Pressure Measurements of Second-Mode Instability in Quiet Hypersonic Flow," AIAA Paper 2008-1153, 2008.

[5] Schneider, S. P., "Development of Hypersonic Quiet Tunnels," *Journal of Spacecraft and Rockets*, Vol. 45, No. 4, July–Aug. 2008, pp. 641–664. doi:10.2514/1.34489

[6] Juliano, T. J., Schneider, S. P., Aradag, S., and Knight, D., "A Quiet-Flow Ludwieg Tube for Hypersonic Transition Research," *AIAA Journal*, Vol. 46, No. 7, July 2008, pp. 1757–1763. doi:10.2514/1.34640

[7] Roediger, T., Jenkins, S., Knauss, H., v. Wolfersdorf, J., Gaisbauer, U., and Kraemer, E., "Time-Resolved Heat Transfer Measurements on the Tip Wall of a Ribbed Channel Using a Novel Heat Flux Sensor, Part 1: Sensor and Benchmarks," *Journal of Turbomachinery*, Vol. 130, No. 1, Jan. 2008, p. 011018. doi:10.1115/1.2751141

[8] Heitmann, D., Roediger, T., Kaehler, C., Knauss, H., Radespiel, R., and Kraemer, E., "Disturbance-Level and Roughness-Induced Transition Measurements in a Conical Boundary Layer at Mach 6," AIAA Paper 08-3951, 2008.

[9] Knauss, H., Roediger, T., Bountin. D. A., Smorodsky, B. V., Maslov, A. A., and Scrulijes, J., "Novel Sensor for Fast Heat Flux Measurements," *Journal of Spacecraft and Rockets*, Vol. 46, No. 2, 2009, pp. 255–265; also AIAA Paper 2006-3637, 2006.

doi:10.2514/1.32011
[10] Mack, L. M., "Boundary-Layer Linear Stability Theory. Special Course on Stability and Transition of Laminar Flow Advisory Group for Aerospace Research and Development," AGARD Rept. No. 709, 1984.
[11] White, F. M., *Viscous Fluid Flow*, McGraw–Hill, New York, 1991.
[12] Anderson, J. D., *Modern Compressible Flow*, McGraw–Hill, New York, 1990.
[13] Zhigulev, V. N., and Tumin, A. M., *The Origin of Turbulence* (in Russian), Science, Novosibirsk, Russia, 1987.
[14] Gaponov, S. A., and Maslov, A. A., *Development of Disturbances in Compressible Flows* (in Russian), Science, Novosibirsk, Russia, 1980.
[15] Stetson, K. F., and Kimmel, R. L., "On Hypersonic Boundary-Layer Stability," AIAA Paper 1992-0737, 1992.

R. Kimmel
Associate Editor